

# Multi-label Scene Classification for Autonomous Vehicles: Acquiring and Accumulating Knowledge from Diverse Datasets

Ke Li, *Graduate Student Member, IEEE*, Chenyu Zhang, *Graduate Student Member, IEEE*, Yuxin Ding, Xianbiao Hu, Ruwen Qin\*, *Member, IEEE*

**Abstract**—Driving scene identification, which assigns multiple non-exclusive class labels to a scene, provides the contextual awareness necessary for enhancing autonomous vehicles’ ability to understand, reason about, and interact with the complex driving environment. As a multi-label classification problem, it is better tackled via multitasking learning. However, directly training a multi-label classification model for driving scene identification through multitask learning presents two main challenges: acquiring a balanced, comprehensively annotated multi-label dataset and balancing learning across different tasks. This paper introduces a novel learning system that synergizes knowledge acquisition and accumulation (KAA) with consistency-based active learning (CAL) to address those challenges. KAA acquires and accumulates knowledge about scene identification from various single-label datasets via monotask learning. Subsequently, CAL effectively resolves the knowledge gap caused by the discrepancy between single-label and multi-label data. An ablation study on our Driving Scene Identification (DSI) dataset demonstrates a 56.1% performance increase over the baseline model pretrained on ImageNet. Of this, KAA accounts for 31.3% of the gain, and CAL contributes 24.8%. Moreover, KAA-CAL stands out as the best performer when compared to state-of-the-art (SOTA) multi-label models on two public datasets, BDD100K and HSD, achieving this while using 85% less data. The DSI dataset and the implementation code for KAA-CAL are available at <https://github.com/KELISBU/KAA-CAL>.

**Index Terms**—Autonomous Vehicle, Driving Scene Identification, Multi-label Classification, Knowledge Distillation, Active Learning

## I. INTRODUCTION

**D**RIVING scene identification involves assigning one or multiple non-exclusive class labels to a scene captured by an onboard camera, selecting from a pre-defined set of categories. For example, driving scenes can be identified based on the weather condition, with possible exclusive categories including clear, overcast, cloudy, raining, and snowing. Scene identification is a crucial function for autonomous vehicles (AVs), as it provides the context or situational awareness for decision-making [1]–[3]. For example, the friction coefficient of the road surface varies, depending on whether the road is dry, wet, snowy, or icy. Identifying driving scenes

based on the road surface condition allows vehicles to adjust the estimations of braking distance and turning speed accordingly, thus improving safety. Scene identification also provides strong support for complex scene reasoning and understanding. From a statistical perspective, contextual awareness enables the estimation of conditional probabilities for random events that influence driving decisions. Conditional probabilities provide more accurate assessments than overall probabilities when the identified conditions are relevant to the event. For example, the probability of a deer suddenly appearing on the road is generally low. However, this probability increases significantly at dawn or dusk, particularly on two-way roads in rural areas. By identifying these conditions, an animal detection system can adaptively adjust its decision threshold, enhancing its ability to respond cautiously.

Driving scene identification is an image classification problem. Due to their complexity, driving scenes can be classified according to multiple scene attributes, resulting in a multi-label classification problem. Each scene attribute is a categorical variable with mutually exclusive yet collectively inclusive classes. Example attributes include weather, time of day, weather-related road condition, road function system, among others. This multi-label image classification problem can be addressed either through monotask or multitask learning. In the monotask learning approach, multiple classification models are trained independently, each classifying driving scenes based on one attribute and thus assigning one class label to an input image. In contrast, multitask learning integrates all the classification tasks into one single model, enabling the simultaneous assignment of multiple non-exclusive class labels to an input image. A multitask model is generally preferred over a set of monotask models because the multitask model is more computationally efficient and, sometimes, can leverage task correlations to improve learning [4], [5].

However, training a multitask model for complex driving scene identification is way more difficult than training a set of monotask models for several reasons. A primary challenge is the lack of a comprehensively annotated multi-label training dataset. In the high-dimensional attribute space, driving scene distribution is highly imbalanced [6], [7]. Some categorical combinations are rare, making it difficult to collect training samples. This data scarcity can cause the model to perform less reliably in low-frequent scenarios. Additionally, a multitask model may struggle to balance learning across tasks, especially when competing gradients arise. These challenges

Ke Li, Chenyu Zhang, and Ruwen Qin are with the Department of Civil Engineering, Stony Brook University, Stony Brook, NY 11794, USA.

Yuxin Ding and Xianbiao Hu are with the Department of Civil and Environmental Engineering, Pennsylvania State University, University Park, PA 16802, USA.

\* Corresponding author: Ruwen Qin, email: ruwen.qin@stonybrook.edu  
Manuscript received Month dd, yyyy; revised Month dd, yyyy.

likely explain why image- and video-level annotations in popular driving scene datasets are either single-labeled (e.g., [8], [9]) or multi-labeled with limited scene attributes (e.g., [10], [11]), and why existing models are predominantly single-label classification models (e.g., [12]–[14]).

The challenge in collecting a balanced multi-label training dataset for complex driving scene identification, combined with the abundance of single-label data sources, motivates the exploration of a novel idea: acquiring knowledge about complex scene identification through monotask learning across diverse single-label datasets. Existing approaches using single-label classification to enhance multi-label scene classification still rely on a multi-label training dataset [6], [7]. Consequently, they are not applicable to the research problem in this paper, which focuses on learning across different datasets. The approach that this paper is interested in is analogous to the learning process of students who study various subjects by adhering to a recurring weekly schedule throughout an academic year. The central idea of the learning process is as follows. A student model learns one classification task from a corresponding single-label dataset at a time in a sequential manner and accumulates the acquired knowledge in a teacher model that serves as a reference for the student model’s continual learning and improvement. This process repeats cyclically until the student model’s performance saturates.

However, learning multi-label classification from single-label datasets through monotask learning must address a domain shift problem, stemming from the discrepancy between the marginal distributions of individual attributes and their joint distribution. This issue could be potentially mitigated by developing an active learning algorithm that selects and annotates some representative samples from the high-dimensional space of scene attributes. Those samples can teach the trained classification model to adapt.

This paper reports an effort in designing and validating the described new deep learning method for complex driving scene identification. In addressing challenges confronted in this study, the paper makes the following contributions:

- A new deep learning system, **Knowledge Acquisition and Accumulation (KAA)**, is proposed for complex driving scene identification.
- In demonstrating KAA, a comprehensive **Driving Scene Identification (DSI)** dataset is constructed, comprising seven single-label subsets, each annotated according to one specific scene attribute.
- An adaptation algorithm, **Consistency-based Active Learning (CAL)**, is developed to address the domain shift problem confronted by KAA.

Remainder of the paper is organized as follows. Section II summarizes recent work related to this study. Then, Section III details the components of the proposed DSI dataset. After that, the learning framework KAA and the adaptation algorithm CAL are introduced in Section IV, with the implementation delineated in Section V. Section VI further reports the experimentation and results. At the end, Section VII concludes the study by summarizing important findings and future research directions.

## II. RELATED WORK

Existing work that builds a foundation for this study includes public driving scene datasets, multi-label scene classification from a computer vision perspective, knowledge distillation, and deep active learning. The most relevant literature is discussed below.

### A. Public Driving Scene Datasets

Various driving video datasets have been developed to support different perception tasks, including scene classification. BDD100K [10] is a large-scale driving video dataset created by the Berkeley DeepDrive (BDD) research group, featuring image-level annotations for six weather conditions, six scene types, and three distinct times of day. Honda Scene Dataset (HSD) [11] contains 80 hours of diverse, high-resolution driving video data clips collected in the San Francisco Bay Area. HSD provides video-level identification of eleven road places, four categories of road environment, and four weather conditions, thereby broadening the diversity of both attributes and classes for scene identification. ROADWork [9] is a large-scale public dataset focused on the identification of work zones with data collected from eighteen cities in the U.S. This dataset also provides fine-grained annotations for instance and semantic segmentation. DENSE++ [4] provides multi-label annotations for environmental conditions including daytime, precipitation, fog, road condition, roadside condition, and scene-setting for 12,997 images collected from Northern Europe. The annotation method is provided, but the labels are not publicly available. WZ-Traffic [8] is a scene dataset with 6,035 single-label images in 20 categories. Other open-source driving datasets, including Cityscapes [15], KITTI [16], and nuScenes [17], are primarily annotated for object detection, semantic segmentation, and instance segmentation tasks.

A review of those datasets reveals that few provide comprehensive annotations for multi-label scene classification. Some datasets provide class labels either at the frame level or the video level, yet they do so based on one or a limited number of attributes of their interest. Additionally, there is no common standard or widely accepted taxonomy for categorizing driving scenes with respect to any given scene attribute, leading to inconsistencies in scene classes across different datasets.

### B. Multi-label Driving Scene Classification

A few studies have tackled the problem of multi-label scene classification in various approaches. Duong et al. [6] developed CF-Net, which uses single-label classifiers to enhance the main multi-label classifier by utilizing feature fusion and stacking. The model was trained on a modified BDD100K dataset with three attributes: location, weather, and time of day. Chen et al. [7] proposed to solve the multi-label scene classification problem by incorporating the single-label training procedure into the multi-label architecture. That allows for addressing the issue of imbalanced categories. Additionally, a deep data integration strategy was utilized to improve the classification ability. RECNet [4] was proposed as a multi-label classification model for identifying environmental conditions. It is a

multitask model that uses the EfficientNet-B2 as the shared backbone and six downstream classifiers to identify all annotated environmental conditions, including daytime, fog, precipitation, road condition, roadside condition, and infrastructure. The study proposed a hierarchical strategy for annotating the environmental conditions, generating a fully annotated dataset DENSE++ for training the multi-label classification model. Prykhodchenko and Skruch [5] also trained a multi-label scene classification model on BDD100K via multitask learning. Data augmentation and balancing strategies were utilized to address the class imbalance issue in the BDD100K dataset.

A review of those studies on multi-label scene classification suggests that multitask learning is a more commonly pursued approach than monotask learning for training such models. Integrating knowledge from single-label classification into multi-label classification models has been shown to be an effective strategy for performance improvement. To the best of our knowledge, no multi-label classification models have been developed through monotask learning from diverse datasets.

### C. Knowledge Distillation

Knowledge distillation (KD) typically utilizes a teacher-student framework to distill the knowledge accumulated in a deep or large model (the teacher) into a smaller or shallow one (the student). It can support the student network’s continual acquisition of scene identification knowledge.

KD methods are generally categorized into three types: response-based KD, where the student directly mimics the teacher’s final predictions; feature-based KD, which transfers knowledge by leveraging features extracted by the teacher; and relation-based KD, which explores relationships between different layers or samples [18]. When both the teacher and student networks are deep, Romero et al. [19] demonstrated that regulating multiple hidden layers of the student network leads to superior performance compared to response-based KD. Ma et al. [20] introduced ARK, a novel framework that accrues and reuses feature-based knowledge to address the challenge of inconsistent annotations in various medical image datasets. Using ARK, a foundation model is constructed for medical image analysis. However, when KD occurs progressively, there is a risk of forgetting previously acquired knowledge. To mitigate this issue, Van de Ven et al. [21] proposed a brain-inspired method that replays internal or hidden representations in continual learning. While sharing some similarities with proposed KAA, ARK primarily focuses on addressing annotation heterogeneity across different datasets.

### D. Deep Active Learning

Deep active learning is typically designed to improve labeling efficiency when faced with the high cost of annotation. Sample selection is guided by an uncertainty-based, diversity-based, or hybrid method.

An uncertainty-based method employs a query strategy to select samples, labeling uncertain samples that provide the most informative data points. Methods such as maximum entropy, margin sampling, least-confidence sampling, and Bayesian Active Learning by Disagreement (BALD) rely

on information derived from a single task [22]. Additionally, a task-agnostic method introduced in [23] integrates a loss prediction module to select top samples of the highest prediction loss within the unlabeled pool, prioritizing them for further downstream tasks.

A diversity-based method selects instances from the unlabeled pool to represent a broad and varied data distribution. Beyond traditional clustering methods like K-means, Core-Set Section [24] computes the distance of features from a designated hint layer within a deep learning model. A greedy search algorithm is employed to iteratively select samples that exhibit the greatest distance from their nearest neighbors until the selection budget is exhausted.

Hybrid methods, including Wasserstein Adversarial Active Learning (WAAL) and Batch Active learning by Diverse Gradient Embeddings (BADGE), effectively mitigate sample redundancy caused by uncertainty-based methods. They also overcome the limitation of diversity-based methods, which often overlook the most informative instances [22]. Hekimoglu et al. [25] introduced a hybrid method for multitask learning, where uncertainty is quantified by an inconsistency score computed as the maximum loss between the initial and refined pairwise task predictions. Simultaneously, a reconstructed feature embedding that condenses information across all tasks is employed to measure the diversity score. The combination of these two components forms the deep active learning basis for multitask learning. However, this approach is limited to multi-label datasets and does not address the domain shift in the high-dimensional feature space that arises when merging multiple single-label datasets.

## III. DRIVING SCENE IDENTIFICATION (DSI) DATASET

The data distribution in the high-dimensional scene attribute space is highly imbalanced. Consequently, some combinations of scene classes are corner cases and challenging to collect data for. This limits the creation of comprehensively annotated datasets to directly support multi-label scene classification. However, collecting data independently from the marginal distributions of scene attributes is relatively easier than sampling from their joint distribution.

This paper introduces DSI, a single-label dataset created to demonstrate the proposed learning systems KAA-CAL. DSI consists of 31,835 scene images sampled from public driving video datasets, including BDD100K [10], HSD [11], and ROADWork Data [9], and is supplemented with additional images from YouTube videos. An overview of the DSI dataset and its statistics are presented in Fig. 1. The dataset is available to the public at <https://github.com/KELISBU/KAA-CAL>.

### A. Driving Scene Attributes and Classes

The DSI dataset consists of  $M$  (7) subsets, denoted as  $\{\mathcal{D}_m\}_{m=1}^M$ . Each subset is annotated according to one unique scene attribute and further partitioned into training (Trn), validation (Vld), and test (Tst) sets:

$$\mathcal{D}_m = \mathcal{D}_m^{Trn} \cup \mathcal{D}_m^{Vld} \cup \mathcal{D}_m^{Tst}. \quad (1)$$

where  $m$  is the index of scene attributes.

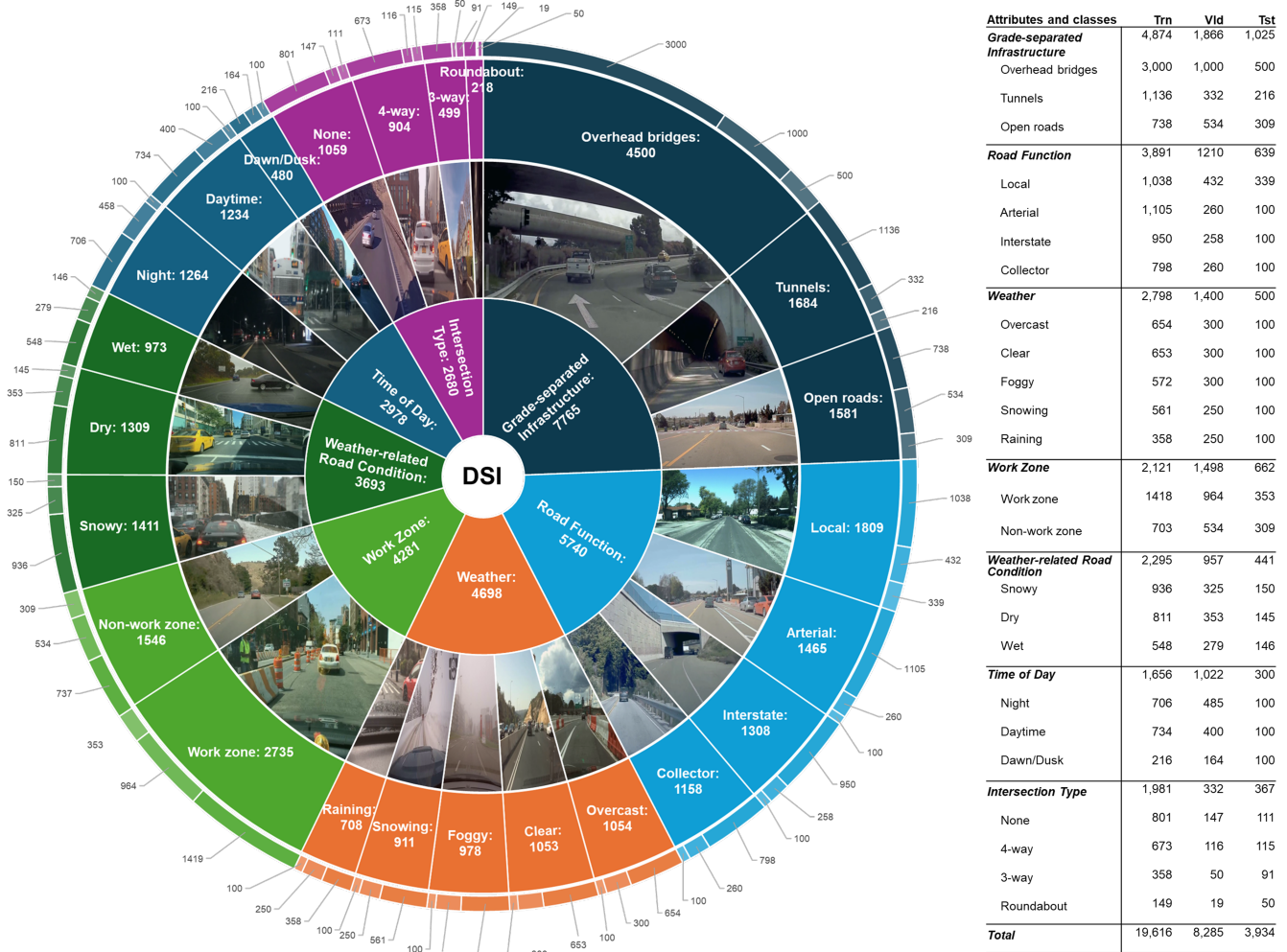


Fig. 1. Overview of the DSI dataset

As illustrated in Fig. 1, these scene attributes include Grade-separated Infrastructure, Road Function, Weather, Work Zone, Weather-related Road Condition, Time of Day, and Intersection Type. In total, DSI provides image-level labels for 24 classes, with each falling exclusively under one of the 7 scene attributes. Classifying driving scenes according to these scene identification attributes offers valuable insights for AVs.

Road segments featuring grade-separated infrastructure, such as bridges and tunnels, often present specific challenges for AVs. Bridges above the road may limit the sensor field of view, cause sudden lighting changes, and introduce gusts of wind. Tunnels, on the other hand, have different lighting conditions, limited visibility, and potential congestion. DSI includes a Grade-separated Infrastructure subset comprising Overhead bridges, Tunnels, and Open roads, totaling 7,765 images. This subset was curated from the HSD dataset using query keywords like “overhead bridge” and “tunnel”. To ensure these structures are visually perceivable, additional query criteria such as “Approaching” and “Entering” were used for data sampling.

Each road type has specific characteristics, such as a speed limit range, traffic density, vehicle type distribution, terrain, and travel purposes. Thus, understanding the road function assists adaptive driving behavior. The US road functional system has not been systematically annotated in public datasets. To address this, the Road Function subset was created by querying with keywords like “road function” on YouTube and sampling every fifth frame from the collected videos. This dataset consists of 5,740 images across 4 classes: Local, Arterial, Interstate, and Collector.

Identification of the weather condition is critical because an adverse weather condition risks driving safety and the performance of visual tasks. The Weather subset includes 4,698 frames sampled from the BDD100K dataset, encompassing Overcast, Clear, Foggy, Snowing, and Raining conditions. To mitigate the issue of data imbalance caused by the rarity of foggy scenes, synthetic images were generated to ensure a more balanced distribution across weather conditions.

Driving safety is a concern in work zones, where construction equipment, temporary barriers, road workers, and other

related facilities are present. Work zones often involve lane closures. Confusion arises when old, not fully removed lane markings mix with new ones, especially for AVs. Identifying work zones allows AVs to adjust their lane position and speed dynamically, minimizing crash risks. The training and validation data of the Work Zone subset mainly come from BDD100K and HSD, and its testing data are primarily from the ROADWork dataset.

The friction coefficient of the road surface changes depending on weather conditions like snow or rain. Identifying these weather-related road conditions allows AVs to adjust their control for better adaptation to the specific surface characteristics. The Weather-related Road Condition subset includes 3,693 images collected from both YouTube and BDD100K, intended for identifying Snowy, Dry, and Wet conditions.

The lighting condition directly impacts the visibility of objects, roads, and the surrounding environment because illumination influences key visual functions like contrast sensitivity, visual acuity, depth perception, and peripheral vision. Consequently, the lighting condition affects human drivers' visual perception and reaction times. It also impacts machine vision due to the affected quality of camera-captured data. For example, nighttime and dawn/dusk images often exhibit increased noise, reduced contrast, and color distortion. The Time of Day subset comprises 2,978 images labeled as Night, Daytime, or Dawn/Dusk, sampled from the BDD100K dataset.

More than half of the combined total of fatal and injury crashes occur at or near intersections due to increased conflict points and complex interactions among vehicles, pedestrians, and other road users. Recognizing the type of intersection allows AVs to anticipate potential conflict points and make informed decisions, such as yielding, stopping, or merging in complex environments. The Intersection Type subset consists of 2,680 images, categorized into four classes: None, 3-way, 4-way, and Roundabout. The data were collected by integrating YouTube videos, which provide roundabout images, along with the HSD and BDD100K datasets, which contribute images of none, 3-way, and 4-way intersections. 3-way and 4-way intersections are typically more noticeable when ego-vehicles are entering the intersection, but less so when approaching or passing through them. Therefore, the query keyword "entering" was used when searching for images of 3-way and 4-way intersections in the HSD dataset.

### B. Diversity and Generalization

Small biases in training data can lead to poor generalization of deep learning models, as a biased dataset may cause the model to learn features that deviate from the intended task [26]. Therefore, the data collection heavily emphasized diversity and generalization to mitigate potential biases. For instance, in the Work Zone subset, data points were sampled across various land use categories (urban and rural areas), road functions, and lighting conditions. This ensures that the DSI dataset provides a good opportunity for learning representations likely encountered in the real world.

## IV. METHODOLOGY

Multi-label driving scene classification involves assigning multiple non-exclusive class labels to each input scene image  $\mathbf{x}$  in the domain  $\mathcal{I} = \{\mathbf{x} | \mathbf{x} \in \mathbb{R}^{3 \times H \times W}\}$ , a set of color images with three color channels, a height of  $H$  pixels, and a width of  $W$  pixels.  $\mathbf{x}$  can be classified based on  $M$  different scene attributes,  $Y_m$ , for  $m = 1, \dots, M$ . Each attribute  $Y_m$  is a categorical variable with its support  $\mathcal{U}_m$  comprising the exclusive classes for this attribute. A multi-label classification model  $\mathcal{C}$  approximates the mapping,  $\mathcal{I} \rightarrow \mathcal{U}_1 \times \dots \times \mathcal{U}_M$ , which estimates the class labels for each scene image  $\mathbf{x}$ :

$$[\hat{\mathbf{y}}_1, \dots, \hat{\mathbf{y}}_M] = \mathcal{C}(\mathbf{x}; \Theta), \quad (2)$$

where  $\hat{\mathbf{y}}_m \in \mathbb{R}^{|\mathcal{U}_m|}$  is the prediction in probability for the one-hot encoded true label  $\mathbf{y}_m \in \mathbb{B}^{|\mathcal{U}_m|}$  of  $\mathbf{x}$ , and  $\Theta$  represents the learnable parameters of the classification model  $\mathcal{C}$ . To build such a model, this section proposes a new deep learning method named KAA-CAL. First, KAA learns a model  $\tilde{\mathcal{C}} = \mathcal{C}(\cdot, \tilde{\Theta})$  that maximizes the classification accuracy in isolated per-attribute identification. Following this, CAL further adapts  $\tilde{\mathcal{C}}$  to become  $\mathcal{C}^* = \mathcal{C}(\cdot, \Theta^*)$  that is proficient in simultaneous all-attribute identification.

### A. Knowledge Acquisition and Accumulation (KAA)

KAA, depicted in Fig. 2, is a deep learning system designed to acquire and accumulate knowledge from various single-label datasets for multi-label driving scene classification. KAA utilizes a teacher-student network architecture. The knowledge acquisition network (KAqN) serves as the student network, responsible for learning new knowledge and consolidating it into the existing knowledge in the learning system. The knowledge accumulation network (KAcN), acting as the teacher network, stores the consolidated knowledge and applies it to guide the student network in continual learning and improvement.

KAqN's deep encoder is trained to attain the knowledge for performing  $M$  downstream tasks, indexed by  $m$ , each focused on classifying the input driving scene image according to one attribute. The overall approach of KAqN is a sequential and cyclical learning process, as outlined in Algorithm 1. A training epoch, indexed by  $t$ , is one learning cycle. During each learning cycle, KAqN goes through  $M$  learning iterations to sequentially learn on these classification tasks, utilizing a dedicated single-label dataset for each task. Mathematically speaking, the current learning iteration  $i$  corresponds to a specific learning cycle  $t$  and learning task  $m$ :

$$\begin{aligned} t &= \lceil i/M \rceil, \\ m &= i - (t - 1)M. \end{aligned} \quad (3)$$

Conversely, the training on task  $m$  within cycle  $t$  is conducted in learning iteration  $i$ :

$$i = (t - 1)M + m. \quad (4)$$

Upon completion of one learning cycle, the newly acquired knowledge is consolidated into the existing knowledge stored in KAcN, forming an updated foundation for continual learning in the subsequent cycle. This cyclical and sequential learning process continues until the stopping criterion is met. KAA's architecture and design are further delineated below.

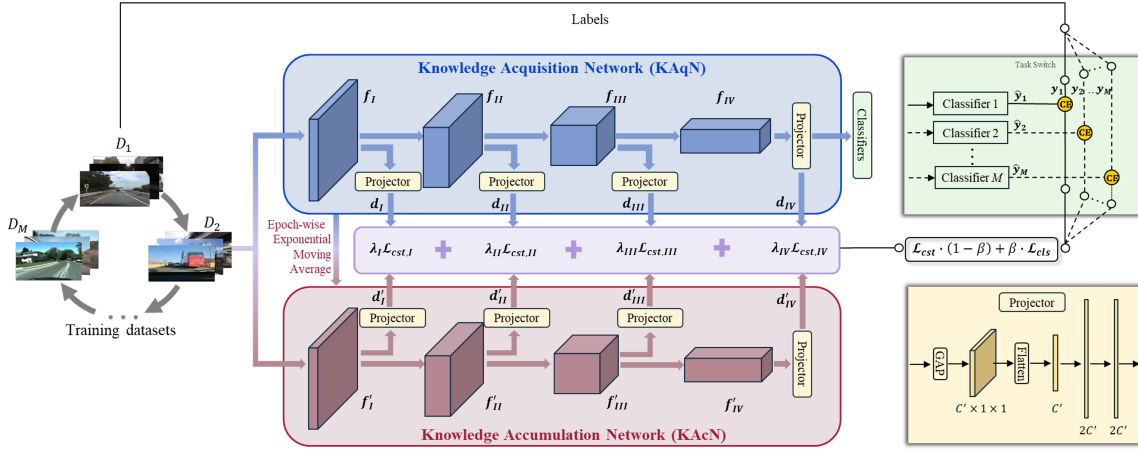


Fig. 2. Overview of the proposed Knowledge Acquisition and Accumulation learning system (KAA)

**Algorithm 1: KAA Algorithm**
**INPUT:**

$\{\mathcal{D}_m \mid m = 1, \dots, M\}$ : the DSI dataset comprising  $M$  single-label subsets

**INITIALIZATION:**

$i \leftarrow 0$ : index of learning iteration

$t \leftarrow 0$ : index of learning cycle

$\theta(0)$ : initial values for KAqN

$\phi_m(0)$ : initial values for classifier  $m$ , for

$m = 1, \dots, M$

$\theta'(0)$ : initial values for KAeN

**CYCLICAL & SEQUENTIAL LEARNING PROCESS:**

$i = 0$

**for** cycle  $t = 1, \dots, T$  **do**

    KAqN acquires new knowledge sequentially:

**for** task  $m = 1, \dots, M$  **do**

$i = i + 1$

        learning classification task  $m$  on dataset  $\mathcal{D}_m$ :

$\theta(i-1)$  is updated to become  $\theta(i)$

$\phi_m(t-1)$  is updated to become  $\phi_m(t)$

**end**

$\theta(Mt)$  is consolidated with  $\theta'(t-1)$ :

$\theta'(t) \leftarrow \frac{\theta(Mt)}{\theta'(t-1)}$

    Termination of the learning process:

**if** stopping criterion is satisfied **then**

$\tilde{t} = t$ ;

**break**

**end**

**end**

**OUTPUT:**  $\tilde{\Theta} \leftarrow \{\theta'(\tilde{t}), \phi_1(\tilde{t}), \dots, \phi_M(\tilde{t})\}$

1) *Knowledge Acquisition*: KAqN utilizes the backbone of a Swin-B [27], a vision transformer pretrained on ImageNet, as the deep feature encoder. The encoder embeds each input image as a feature map for the downstream classification tasks. Specifically, Swin-B processes an input scene image with a resolution of  $244 \times 244$  by first partitioning it into non-

overlapping  $4 \times 4$  patches. It then sequentially encodes these patches into a feature map through four stages. Each stage applies either a linear embedding (LE) or a patch merging (PM) layer, followed by multiple Swin Transformer (ST) blocks:

$$\begin{aligned} \mathbf{f}_I &= \text{ST}(\text{ST}(\text{LN}(\mathbf{x}; \theta_{I,0}^{\mathcal{E}}; \theta_{I,1}^{\mathcal{E}}; \theta_{I,2}^{\mathcal{E}}), \\ \mathbf{f}_{II} &= \text{ST}(\text{ST}(\text{PM}(\mathbf{f}_I; \theta_{II,0}^{\mathcal{E}}; \theta_{II,1}^{\mathcal{E}}; \theta_{II,2}^{\mathcal{E}}), \\ \mathbf{f}_{III} &= \text{ST}(\dots \text{ST}(\text{PM}(\mathbf{f}_{II}; \theta_{III,0}^{\mathcal{E}}; \theta_{III,1}^{\mathcal{E}}; \theta_{III,6}^{\mathcal{E}}), \\ \mathbf{f}_{IV} &= \text{ST}(\text{ST}(\text{PM}(\mathbf{f}_{III}; \theta_{IV,0}^{\mathcal{E}}; \theta_{IV,1}^{\mathcal{E}}; \theta_{IV,2}^{\mathcal{E}}). \end{aligned} \quad (5)$$

Here,  $\theta^{\mathcal{E}}$  designates all the learnable parameters of KAqN's deep encoder in Eq. (5). The extracted feature maps have the following dimensions:  $\mathbf{f}_I \in \mathbb{R}^{128 \times 56 \times 56}$ ,  $\mathbf{f}_{II} \in \mathbb{R}^{256 \times 28 \times 28}$ ,  $\mathbf{f}_{III} \in \mathbb{R}^{512 \times 14 \times 14}$ , and  $\mathbf{f}_{IV} \in \mathbb{R}^{1024 \times 7 \times 7}$ . That is, the encoder in Eq. (5) progressively reduces the spatial resolution of the input scene image while increasing the depth (number of channels) of the feature maps.

Then, four projectors independently embed the individual feature maps derived from each stage as feature vectors,

$$\mathbf{d}_s = \text{MLP}(\text{Flatten}(\text{GAP}(\mathbf{f}_s)); \theta_s^{\mathcal{P}}), \quad (6)$$

for  $s = I, \dots, IV$ . Here,  $\theta^{\mathcal{P}}$  designates the learnable parameters for the four projectors. Eq. (6) states that each projector first downsamples the input feature map  $\mathbf{f}_s$  through global average pooling (GAP), reducing its spatial dimensions to 1 while keeping the number of channels unchanged. Then, the downsampled feature map is flattened (Flatten) as a vector, which then goes through a multi-layer perceptron (MLP) with two hidden layers. The resulting feature embeddings are  $\mathbf{d}_I \in \mathbb{R}^{256}$ ,  $\mathbf{d}_{II} \in \mathbb{R}^{512}$ ,  $\mathbf{d}_{III} \in \mathbb{R}^{1024}$ , and  $\mathbf{d}_{IV} \in \mathbb{R}^{2048}$ .

Finally, the feature embedding from the last stage,  $\mathbf{d}_{IV}$ , flows into classifier  $m$ , which is active in the current learning iteration, to predict the probability distribution for the classes of attribute  $m$ :

$$\hat{\mathbf{y}}_m = \text{SM}(\text{FC}(\mathbf{d}_{IV}; \phi_{\text{FC},m}); \phi_{\text{SM},m}). \quad (7)$$

The fully-connected (FC) layer of the classifier reduces the dimension of feature embedding  $\mathbf{d}_{IV}$  to match the class size of attribute  $m$ , and the softmax operator (SM) normalizes

the output as the probability distribution over classes.  $\phi_m$  represents the learnable parameters of classifier  $m$  in Eq. (7).

KAqN's performance on the classification task  $m$  in any learning iteration is evaluated by calculating the corresponding cross-entropy loss:

$$\mathcal{L}_{cls,m} = -\mathbf{y}_m \cdot \log \hat{\mathbf{y}}_m, \quad (8)$$

where  $\cdot$  denotes the inner product of the one-hot encoded ground truth class label,  $\mathbf{y}_m$ , and the predicted probability distribution over classes,  $\hat{\mathbf{y}}_m$ . The prediction loss in Eq. (8) is part of the total loss (to be introduced in Eq. (15)) for guiding the modeling training.

Within a learning cycle  $t$ , KAqN learns classification tasks one at a time, using a dedicated single-label dataset for each task. In completing a learning iteration described in Eqs. (5, 6, 7, 15), KAqN's parameter values are updated:

$$\theta(i) \xleftarrow{\text{monotask learning}} \theta(i-1), \quad (9)$$

and so the classifier for that task:

$$\phi_m(t) \xleftarrow{\text{monotask learning}} \phi_m(t-1). \quad (10)$$

$\theta$  in Eq. (9) is the collection of the encoder's parameters  $\theta^E$  and the projectors' parameters  $\theta^P$ . At the end of learning cycle  $t$ , KAqN completes its training on all the  $M$  tasks. The resulting parameter values,  $\theta(Mt)$ , embed the acquired new knowledge about the driving scene classification.

2) *Knowledge Accumulation*: Knowledge acquired by KAqN in the cyclical training process is accumulated in KAcN. Fig. 2 shows that KAcN's network architecture is identical to KAqN. The feature map extracted in each stage of the KAcN's encoder is  $\mathbf{f}'_s$ , which is further embedded as a feature vector  $\mathbf{d}'_s$ , for  $s = 1, \dots, IV$ . For simplicity,  $\theta'$  designates all the learnable parameters of KAcN. The identical network architecture of KAcN and KAqN greatly simplifies the process of knowledge accumulation delineated as below.

Upon the completion of the learning cycle  $t$ , KAA needs to consolidate the new knowledge acquired by KAqN,  $\theta(Mt)$ , with the previously learned knowledge stored in KAcN,  $\theta'(t-1)$ . For this consolidation, KAA adopts exponential moving average (EMA), a temporal mechanism for accumulating knowledge from cyclical learning [28]:

$$\theta'(t) = \alpha(t)\theta'(t-1) + (1 - \alpha(t))\theta(Mt), \quad (11)$$

where  $\alpha(t)$  is the stability coefficient, a real-valued parameter within the range  $[0.9, 1]$ .  $\alpha(t)$  determines the proportion of previously learned knowledge to retain in cycle  $t$ .

KAA, as a learning system, needs to keep a balance between retaining already learned knowledge and acquiring new knowledge, a phenomenon called stability-plasticity tradeoff in neuroscience [29], incremental learning [30], and continual learning [31]. If KAA is too stable, it will struggle to learn new knowledge effectively. Conversely, if it is too plastic, it risks forgetting important knowledge that has already been acquired. This paper designs a cosine scheduler for progressively updating the stability coefficient  $\alpha(t)$  in Eq. (11) from 0.9 to 1 in the cyclical learning process:

$$\alpha(t) = 0.9 + 0.05 [1 - \cos(t\pi/T)], \quad (12)$$

where  $T$  is the maximum learning cycles for KAA. Eq. (12) indicates that  $\alpha(t)$  is a monotonically increasing function. That is, in the early phases of learning, KAA leans toward plasticity, allowing itself to rapidly absorb new knowledge. In the later phases, it prioritizes stability and thus becomes more conservative in absorbing new knowledge to prevent the disruption of the established cognitive capability.

3) *Knowledge Retention*: The cyclical nature of training can cause catastrophic forgetting, thus impeding continual learning and improvement. This issue can be effectively addressed by setting the accumulated knowledge as the reference for the subsequent knowledge acquisition. KAA achieves this through feature-based KD, which penalizes stage-wise discrepancies between the feature embedding extracted by KAqN,  $\mathbf{d}_s(i)$ , in each learning iteration and the corresponding feature embedding derived by KAcN,  $\mathbf{d}'_s(t-1)$ . The penalty is calculated as the mean squared error (MSE):

$$\mathcal{L}_{cst,s}(i) = \frac{1}{|\mathbf{d}_s|} \|\mathbf{d}_s(i) - \mathbf{d}'_s(t-1)\|_2^2, \quad (13)$$

for stages  $s = I, \dots, IV$ . This particular KD design fully leveraging the advantages of network depth has been shown to be effective [19].

Then, the overall consistency loss is the weighted sum of stage-wise consistency losses:

$$\mathcal{L}_{cst}(i) = \sum_{s=1}^{IV} \lambda_s \mathcal{L}_{cst,s}(i), \quad (14)$$

where  $\lambda_s$  is the coefficient for stage  $s$ . In this study,  $\lambda_s$  is 1 for all stages, meaning equal weights are assigned across stages.

4) *Loss Function as Learning Guidance*: KAA uses the consistency loss calculated in Eq. (14) as a regularization term for training KAqN to ensure the new knowledge acquisition is based on already attained knowledge. Therefore, the per-sample loss function in learning iteration  $i$  can be formulated as the weighted sum of the prediction loss and the consistency loss:

$$\mathcal{L}_{tot}(i) = \beta(i)\mathcal{L}_{cls}(i) + (1 - \beta(i))\mathcal{L}_{cst}(i), \quad (15)$$

where  $\beta(i)$ , a real-valued parameter in the range  $[0, 1]$ , is the performance-based acquisition-retention indicator (PARI) for balancing the acquisition of new knowledge and the retention of already attained knowledge.  $\beta(i)$  is designed to be adjusted dynamically with respect to the learning needs. Lower performance anticipated for KAqN on the task in learning corresponds to a greater need for continual learning and improvement on this task. Therefore,  $\beta(i)$  is designed as a monotonically decreasing function of the estimated task performance,  $\hat{p}(i)$ :

$$\beta(i) = (1 - \hat{p}(i)^\psi)^{1/\psi}, \quad (16)$$

where  $\psi > 1$  is a real-valued parameter defining the shape of the curve. In this study,  $\psi$  is set to be 4.

In Eq. (16),  $\hat{p}(i)$ , the estimated classification accuracy of KAqN in learning iteration  $i$ , is obtained based on an EMA process:

$$\hat{p}(i) = \omega \hat{p}(i-M) + (1 - \omega)p(i-M), \quad (17)$$

where  $\hat{p}(i - M)$  is the estimated accuracy of KAqN for the last learning cycle and  $p(i - M)$  is the accuracy that KAqN actually achieved. When a prior measurement or estimation is not available, a default value,  $\hat{p}(0)$ , representing KAqN's initial (low) performance, is used as a substitute. The parameter  $\omega$  is set to be 0.9 in this study, meaning that the performance estimation puts more weight on the long-term trend than the most recent observation.

Summing the loss function in Eq. (15) over all the training data yields the total training loss. By minimizing this loss with respect to KAqN's learnable parameters in each learning iteration and across learning cycles, the classification model defined in Eq. (2) is optimized. The resulting classification model  $\tilde{C}$ , described in Algorithm 1, is a foundation model for driving scene identification.

### B. Consistency-based Active Learning (CAL)

KAA learns to perform multi-label scene classification through monotask learning across different single-label datasets. While simplifying data collection and reducing learning complexity, this approach encounters a domain shift issue. Precisely, the class label distributions of single-label datasets represent the marginal probabilities of individual attributes, different from their joint probabilities. A similar domain shift occurs in the extracted features. Consequently, the resulting classification model can make mistakes when it is tested on samples drawn from the joint distribution of driving scenes.

This paper proposes CAL to tackle the aforementioned issue, which seeks to accomplish multi-label classification in real-world scenarios in a cost-effective manner. Eventually, the classification model obtained by KAA via monotask learning will adapt to multitask learning, thereby achieving satisfactory performance for multi-label classification.

Fig. 3 illustrates the overall approach of the proposed CAL. A multi-label test sample,  $\mathcal{D}^T$ , is prepared, representing the driving scene distribution in the joint space of scene attributes. As outlined in Fig. 3, a stratified sampling strategy (Stf) is implemented, which randomly samples  $\kappa$  test images per class from DSI's test sets:

$$\mathcal{D}^T = \cup_{m=1}^M \text{Stf}(\mathcal{D}_m^{\text{Tst}}; \mathcal{U}_m, \kappa), \quad (18)$$

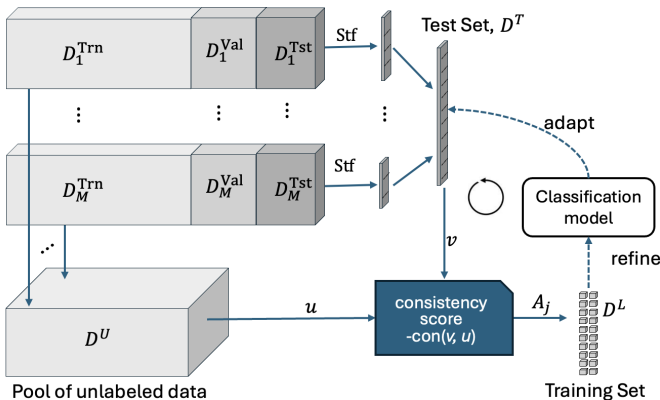


Fig. 3. Schematic diagram for Consistency-based Active Learning (CAL)

which is then fully annotated with respect to all  $M$  attributes.

Then, a labeled training set  $\mathcal{D}^L$  needs to be obtained to adapt the classification model for multitask learning over iterations. Although the ground truth labels for the training set  $\mathcal{D}_m^{\text{Trn}}$  were seen by task  $m$ , other tasks have never seen these labels. Therefore, the union of DSI's training sets forms an "unlabeled" pool,

$$\mathcal{D}^U = \cup_{m=1}^M \mathcal{D}_m^{\text{Trn}}, \quad (19)$$

from which training samples can be selected and prepared according to Algorithm 2.

CAL, as outlined in Fig. 3 and Algorithm 2, searches the unlabeled pool  $\mathcal{D}^U$  for data points that are similar to those in the test set  $\mathcal{D}^T$ . A consistency function,  $\text{con}(v, u)$ , is defined to quantify the similarity between any image in the test set  $v \in \mathcal{D}^T$  and any one in the unlabeled pool  $u \in \mathcal{D}^U$ :

$$\text{con}(v, u) = -\|v, u\|_{d'_{v,2}}, \quad (20)$$

where  $\|\cdot, \cdot\|_{d'_{v,2}}$  measures the Euclidean distance between two data points based on their final-stage feature embeddings. Thereby, for any image in the test set  $v \in \mathcal{D}^T$ , its nearest neighbor (i.e., the corresponding image in the unlabeled pool which is most similar to it) is found:

$$\bar{u} = \arg \max_{u \in \mathcal{D}^U} \text{con}(v, u). \quad (21)$$

Then, these unlabeled images are ranked in decreasing order of their consistency score:

$$\text{con}(v^{(1)}, \bar{u}^{(1)}) > (v^{(2)}, \bar{u}^{(2)}) > \dots \quad (22)$$

to prioritize them for annotation. Following the ranking, the top  $b_j$  unlabeled images with the highest consistency scores are selected for annotation:

$$\mathcal{A}(j) = \{\bar{u}^{(1)}, \dots, \bar{u}^{(b_j)}\}, \quad (23)$$

where  $b_j$  is the annotation budget in iteration  $j$ . After that,  $\mathcal{A}(j)$  is moved from the unlabeled pool to the labeled training set,  $\mathcal{D}^L$ :

$$\mathcal{D}^L \leftarrow \mathcal{D}^L \cup \mathcal{A}(j), \quad (24)$$

$$\mathcal{D}^U \leftarrow \mathcal{D}^U \setminus \mathcal{A}(j). \quad (25)$$

The dataset  $\mathcal{D}^L$  is used to refine the classification model into a multitask model.

In refining the classification model, the focal loss is evaluated for each data point in the training set  $\mathcal{D}^L$  to focus on hard samples for each task,

$$\mathcal{L}_{MT} = - \sum_{m=1}^M \mathbf{y}_m \cdot ((1 - \hat{\mathbf{y}}_m)^{\gamma_m} \odot \log \hat{\mathbf{y}}_m), \quad (26)$$

where  $\odot$  stands for the element-wise product,  $\cdot$  is the dot product, and  $\gamma_m$  is the focusing parameter for task  $m$ , which is set to 1 here. The total loss of the multitask learning process is obtained by summing up this loss across in Eq. (26) across all data points in  $\mathcal{D}^L$ , which guides the model refinement iteratively:

$$\Theta'(j) \xleftarrow{\text{multitask learning}} \Theta'(j-1), \quad (27)$$

where  $\Theta'(0) = \tilde{\Theta}$ . This process can go for multiple iterations until satisfaction, resulting in the optimized classification model  $\mathcal{C}^*$  parameterized with  $\Theta^*$ .

---

**Algorithm 2: CAL Algorithm**


---

**INPUT:** $\mathcal{D}^U$ : Unlabeled pool $\mathcal{D}^T$ : Test dataset $b_j$ : Budget for adaptation iteration  $j$  $N_{\text{CAL}}$ : Maximum iterations**INITIALIZATION:** $\mathcal{D}^L = \emptyset$ : initial labeled training set $\Theta'(0) = \tilde{\Theta}$ : initial learnable parameters**CONSISTENCY ACTIVE LEARNING:****for**  $j = 1, \dots, N_{\text{CAL}}$  **do**    compute consistency score  $\text{con}(v, \bar{u}), \forall v \in \mathcal{D}^T$ ;     $\mathcal{A}(j)$  comprises  $b_j$  samples from  $\mathcal{D}^U$  with top consistency scores, labeled by the Oracle;    add  $\mathcal{A}(j)$  to the labeled dataset:         $\mathcal{D}^L \leftarrow \mathcal{D}^L \cup \mathcal{A}(j)$ ;    remove  $\mathcal{A}(j)$  from unlabeled dataset:         $\mathcal{D}^U \leftarrow \mathcal{D}^U \setminus \mathcal{A}(j)$ ;

train the classification model for multitasking:

 $\Theta'(j) \xleftarrow{\text{multitask learning}} \Theta'(j-1)$ .    **if** *stopping criterion is satisfied* **then**         $j^* = j$ .        **break**    **end****end****Output:**  $\Theta^* = \Theta'(j^*)$ 

## V. IMPLEMENTATION DETAILS

The proposed KAA-CAL learning system was implemented using PyTorch 1.10.0 on a server equipped with an Nvidia Tesla V100 featuring 32 GB of memory. Model training utilized the AdamW optimizer, a batch size of 32, and a maximum of 100 training epochs. Input images were resized to  $224 \times 224$  and augmented with random rotations, crops, and pixel normalization.

### A. KAA Implementation

The deep encoder for KAA in Eq. (5) was initialized by loading the weights pretrained on ImageNet-22k [32]. The projectors in Eq. (6) and the classifiers in Eq. (7) were initialized using the default Xavier initialization method [33]. Then, learnable model parameters were progressively optimized using the method delineated in Algorithm 1.

The learning rate for KAA implementation was adjusted in a two-phase approach. It began with a 10-epoch warm-up, where the learning rate linearly increased from an initial value of  $1e-6$  to  $5e-4$ . Following this, the learning rate decayed to a final value of  $1e-5$  using a cosine schedule. Upon convergence at the end of all training epochs, the model from the final epoch was chosen as the ultimate model.

### B. CAL Implementation

In implementing CAL, a per-iteration budget ( $b_j$ ) of 200 images (approximately 1% of the single-label training data in DSI) was allocated for annotating the data selected using Algorithm 2. This process ran for up to five iterations to evaluate the efficiency of CAL.

The data annotation process confronted a challenge. Not all images can be reliably annotated with all the seven driving scene attributes. For example, the weather condition in some night-time images was hard to identify, and annotators were not always confident about the road function for some scene images. When a reliable label was unavailable, a class label of “-1” was assigned. Critically, these labels were excluded from the loss function evaluation to ensure training integrity.

Aiming to retain knowledge learned from KAA, the first three stages of the deep encoder were frozen for finetuning multitask classification. The learning rate scheduler was similarly configured for the CAL implementation: it began with a 10-epoch warm-up, with the learning rate linearly increasing from  $1e-6$  to  $1e-3$ . After that, the learning rate decayed to a final value of  $1e-5$  based on a cosine schedule.

## VI. EXPERIMENTS AND RESULTS

This section presents experimental studies, aiming to verify the merits of the proposed KAA-CAL learning system. First, Subsections A-C will assess the advantages of KAA’s designs and the performance of the resulting foundation model. Then, Subsection D will evaluate the efficiency and effectiveness of CAL that adapts the foundation model for multitasking. Upon those analyses, an ablation study will be further performed in Subsection E to quantify the respective and joint contributions of learning and adaptation, supplemented by examples presented in Subsection F. In the end, Subsection G will compare the multi-label classification model attained via KAA-CAL to its variants and state-of-the-art (SOTA) multitask models on public datasets.

### A. Deep Encoder Selection

Vision transformers (ViT) demonstrate unique advantages over convolutional neural networks (CNNs) in learning deep features for image classification tasks. In selecting a deep encoder for the KAA-CAL learning system, the study compared SOTA transformer-based models, including Swin-S, Swin-B, ViT-B, and ViT-L. This comparison spanned the seven independent image classification tasks, evaluating models from the perspectives of both classification accuracy and model complexity. The results are summarized in TABLE I, with the highest accuracy achieved on each task being bolded.

As expected, Swin-B outperforms Swin-S on all seven tasks, and the same pattern holds for ViT-L compared to ViT-B. This confirms that the more complex versions of the models (Swin-B and ViT-L) achieve better performance than their less complex counterparts. While both are powerful vision transformers, Swin transformers address several limitations of the original ViT, exhibiting improved computational efficiency and the capability for multi-scale feature learning. TABLE I shows that Swin-B outperformed ViT-L on five out of seven

TABLE I  
CLASSIFICATION ACCURACY (%) COMPARISON OF VISION TRANSFORMERS AS THE DEEP ENCODER IN MONOTASK LEARNING

	Swin-B	Swin-S	ViT-B	ViT-L
<b>MODEL COMPLEXITY</b>				
FLOPs (G)	15.4	8.7	17.6	76.9
The number of parameters (M)	88	50	86	307
<b>ACCURACY (%)</b>				
Time of Day	<b>99.6</b>	91.3	89.3	96.0
Weather	<b>92.2</b>	92.0	90.9	92.1
Weather-related Road Condition	<b>98.4</b>	97.7	96.7	96.6
Road Function	<b>99.8</b>	99.2	95.4	95.8
Intersection	88.6	86.9	93.4	<b>95.8</b>
Work Zone	<b>95.2</b>	87.9	88.5	90.2
Grade-separated Infrastructure	94.6	93.7	97.2	<b>98.4</b>
Average	<b>95.5</b>	92.7	93.4	95.0

tasks with a margin ranging from 0.1% to 4.9%. Importantly, the FLOPs for Swin-B are only 20% of ViT-L. Given the highest average accuracy and more affordable model complexity, Swin-B is chosen as the deep encoder architecture for the classification model.

*B. Effectiveness of Stage-wise Knowledge Distillation*

Sections IV-A3 and IV-A4 explained that, when KAqN continues acquiring new knowledge, KAA retains the already acquired knowledge accumulated in KAcN through stage-wise feature-based KD, and the intensity of this regularization is moderated by PARI. To demonstrate the effectiveness of the knowledge retention design for KAA, an ablation study about KD was performed with results summarized in TABLE II.

The Baseline model in TABLE II is learned solely by a student network because both stage-wise KD and PARI are removed. It results in an average accuracy of 92.7%, representing a 2.5% decrease compared to our model (Model IV). It is suspected that the gap will increase when the KAA attempts to acquire more diverse knowledge from many datasets.

Model I adds last-stage KD to the baseline model, analogous to a teacher who provides less guidance to the student’s learning. This model achieves a negligible performance gain of merely 0.1%. Conversely, Model III incorporates stage-wise KD into the baseline model, leading to a substantial average accuracy increase of 1.8%. This comparison highlights the importance of stage-wise KD, especially since features

TABLE II  
EFFECTIVENESS OF KNOWLEDGE RETENTION THROUGH STAGE-WISE FEATURE-BASED KNOWLEDGE DISTILLATION

Model	Last-stage KD	Stage-wise KD	PARI	Avg. (%)
Baseline				92.7
Model I	✓			92.8
Model II	✓		✓	94.0
Model III		✓		94.5
Model IV (Ours)		✓	✓	<b>95.2</b>

of different scales contain comprehensive information about driving scenes.

Model II augments last-stage KD with PARI, which improves average accuracy by 1.2% over Model I. Similarly, Model IV pairs PARI with stage-wise KD, increasing Model III’s well-performed average accuracy by an additional 0.7%. These observations verify the effectiveness of dynamically adjusting the weight for new knowledge acquisition according to specific learning needs, regardless of the KD method.

*C. Performance of the Foundation Model*

After verifying the strengths of KAA’s architecture design, the experimental study continued to assess the resulting foundation model’s performance. Fig. 4 compares the foundation model to the seven individual monotask models. As illustrated, the foundation model is comparable to the individual monotask models in task accuracy, with variations ranging from -3.9% to 3.2% across the seven tasks. Specifically, the foundation model is 3.2% more accurate than the monotask model for identifying Grade-separated Infrastructure. However, the foundation model’s accuracy in identifying Work Zone is 3.9% lower. This drop can be attributed to the challenge of image-level classification in capturing the fine-grained features critical for the identification of scenes within work zones, such as safety cones and work zone signs. In contrast, approaches based on object detection or semantic segmentation [34], [35] are generally more capable of detecting such localized features. For the remaining five tasks, their performance differences are within  $\pm 1\%$ . The foundation model can substitute for individual models dedicated to different classification tasks, as its comparable performance demonstrates.

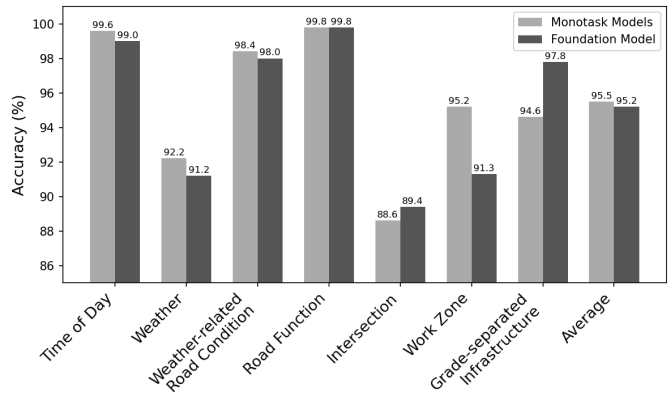


Fig. 4. Comparison of the foundation model with the seven monotask models in terms of classification accuracy

*D. Effectiveness of Consistency-based Active Learning*

As introduced in Section IV-B, CAL is designed to adapt the foundation model to multitask learning, addressing the limitations inherent in KAA’s monotask learning approach. To demonstrate its effectiveness, CAL was compared to its variants and SOTA deep active learning methods, detailed as follows.

- **Ran-I.** In this approach, the deep encoder for the classification model is initialized with the weights pretrained on ImageNet-22k. Samples are randomly selected from each class within the unlabeled pool  $\mathcal{D}_U$  and subsequently annotated for training the model. Compared to CAL, Ran-I does not leverage the driving scene knowledge offered by the foundation model, nor does it employ the feature consistency-based criterion for sampling.
- **Ran-D.** This approach uses the same sampling method as Ran-I, but it adopts the foundation model as its deep encoder. During training, the encoder’s first three stages were frozen.
- **Core-Set-I** [24]. This is a diversity-based active learning approach proposed in [24]. It’s deep encoder is initialized with the weights pretrained on ImageNet. In the first iteration, the model is refined with a starting training set of  $b_1$  samples taken from the unlabeled data pool ( $\mathcal{D}^U$ ), helping expose the encoder to some multi-label training data. After that, in each subsequent iteration, a k-Center-Greedy strategy selects additional diverse samples that represent various clusters in the unlabeled pool.
- **LLAL-I** [23]. This active learning approach follows the same initialization as Core-Set-I, but it introduces an additional loss prediction component developed in [23]. This component is learnable, and it estimates a pseudo-loss value for each sample, aiming to approximate the true task loss. During sample selection from the unlabeled pool, the module prioritizes samples with the highest pseudo-loss values, under the assumption that they represent the most informative samples to learn from.

Fig. 5 compares the proposed CAL method with those introduced above, presenting both the task-level accuracy (a-g) and the average accuracy (h). The plots illustrate test accuracy values before adaptation (the training set  $\mathcal{D}^L$  has 0% labeled data from  $\mathcal{D}^U$ ) and over five iterations of adaptation ( $\mathcal{D}^L$  consists of 1% to 5% of data sampled from  $\mathcal{D}^U$ ). Prior to adaptation for multitask learning, models initialized

with the foundation model’s weights (i.e., CAL and Ran-D) demonstrate a higher average accuracy than those initialized with weights pretrained on ImageNet (i.e., Ran-I, LLAL-I, and Core-set-I), with a margin of 31.3%. The performance gap between these two groups before model adaptation highlights the benefit of utilizing the foundation model for driving scene identification, as it possesses specialized knowledge relevant to this application.

After the first iteration, while all methods improve their task performance, CAL is the top one. It surpasses the best competing method’s accuracy by a significant margin of 3.3% to 10.0% across all tasks, except for the task of identifying Time of Day (Fig. 5(a)). Effectively, CAL brings the classification model’s average accuracy up to 86.2% after just one iteration of adaptation. With another iteration, CAL boosts the average accuracy to 90.1%, with task accuracy ranging from 83.6% to 96.3%. Through additional iterations, CAL further enhances the accuracy for identifying Weather and Road Function, thus increasing the average accuracy to 92.7%. Figure 5(h) reveals CAL’s superior performance and cost-effectiveness. It consistently outperforms the best competing method in every iteration, with margins ranging from 5.0% to 12.9%. Importantly, CAL has achieved its major improvements in just two iterations, while all other methods require more iterations and so more training data for adaptation.

Ran-D and CAL differ in their sampling strategies. Ran-D uses a simple stratified random sampling strategy, whereas CAL samples data based on features consistency measurement between unlabeled data and the test set. CAL consistently improves task accuracy over iterations, whereas Ran-D lowers the accuracy in identifying Road Function and Grade-separated Infrastructure. Moreover, CAL achieves a higher saturated accuracy than Ran-D on all tasks. Consequently, CAL clearly dominates Ran-D in Fig. 5(h), demonstrating the importance of CAL’s selective sampling strategy.

Ran-I, LLAL-I, and Core-Set-I do not benefit from the knowledge attained by the foundation model. Therefore, they

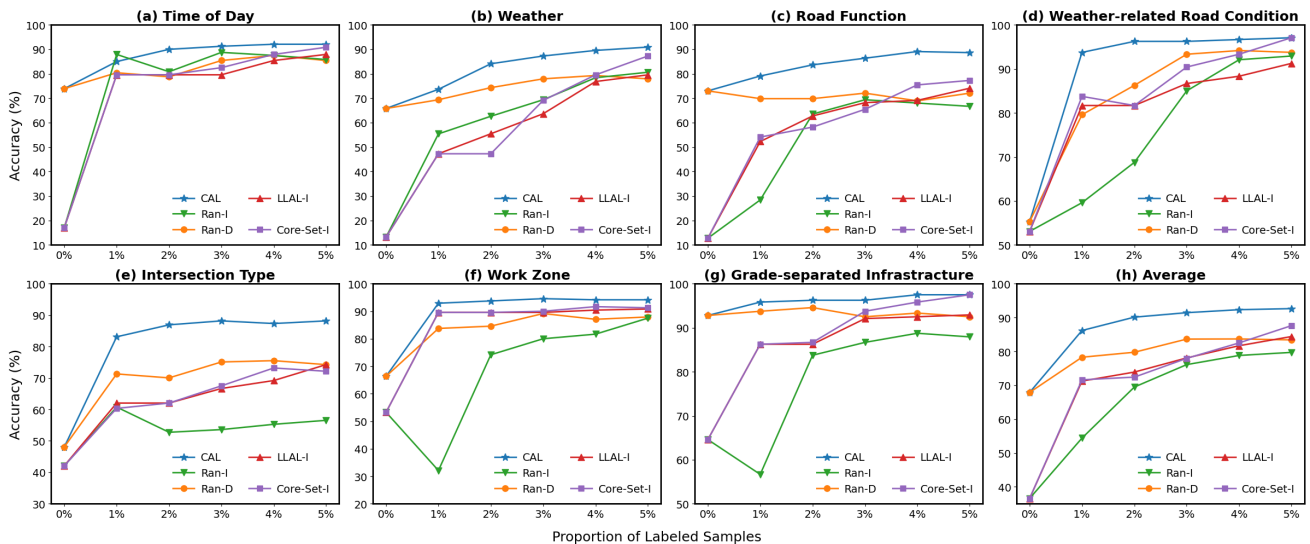


Fig. 5. Comparison of active learning methods in terms of task and average accuracies (%)

need more iterations and so more annotation cost than CAL to improve task performance. Among those methods, Core-Set-I seems the most competitive. After five iterations, Core-Set-I reached task accuracy comparable to CAL’s in identifying Weather-related Road Condition and Grade-separated Infrastructure, but CAL still beat Core-Set-I on the remaining five tasks by a margin ranging from 1.3% to 13.9%. Consequently, Core-Set-I’s average accuracy after five iterations is still 5% lower than that of CAL. CAL’s superior efficiency and consistently good performance across all tasks, as compared to Core-Set-I, highlight the importance of leveraging the foundation model’s knowledge obtained through KAA.

Observations from Fig. 5 also indicate that the CAL method significantly benefits from the foundation model. The foundation model not only sets up a higher starting point for adaptation but also allows CAL to utilize its superior feature extraction ability to search and identify new training data from the unlabeled pool for ongoing learning and refinement. That is, a suitable active learning method, combined with a powerful foundation model, is the underlying reason for the efficiency and effectiveness of model adaptation.

E. Ablation Study

KAA and CAL have now been verified as advantageous designs for a learning system. KAA builds a foundation model for driving scene identification by acquiring and accumulating knowledge from different single-label datasets via monotask learning. The CAL module then adapts this foundation model for multitasking. An ablation study was conducted to gauge their respective contributions, with results summarized in TABLE IV.

The baseline model in this experimentation is a multitask classification model whose deep encoder is the Swin-B pretrained on ImageNet. This baseline model achieves task accuracies ranging from 17.1% to 64.4%, resulting in an average accuracy of 36.6%. The low accuracy observed indicates a lack of knowledge regarding driving scene identification.

Adoption of the foundation model as the deep encoder boosts the average accuracy to 67.9%, representing a substantial increase of 31.3%. This gain is attributed to the comprehensive knowledge regarding driving scenes acquired by KAA from diverse single-label datasets. For instance, the accuracy in identifying Road Function, a unique attribute specific to driving scenes, had an increase of 60.3%. Furthermore, the task accuracies for identifying the environmental attributes, Time of Day and Weather, each rise by over 50%. Consequently, the task accuracies now span from 48.1% to

92.8%. However, there is still clear room for improvement. The gains in identifying Weather-related Road Condition and Intersection are limited, primarily due to the shift in data distribution in real-world scenarios compared to the marginal distributions in the single-labeled datasets.

CAL, designed to address the limitation of KAA’s monotask learning approach, effectively improves the average accuracy to 90.1% with only two iterations, corresponding to another increase of 22.2%. At the task level, accuracies have reached the range from 83.6% to 96.3%. With three additional iterations, the task accuracies in identifying Weather and Road Function are improved by at least 5%, further boosting the average accuracy to 92.7%. The efficient improvement in the accuracy of multitask-based driving scene classification demonstrates CAL’s effectiveness in integrating knowledge acquired through monotask learning on single-label datasets into knowledge suitable for multi-label scene identification.

F. Driving Scene Identification Examples

To supplement the ablation study, seven examples (a-g) are further provided, with their corresponding results detailed in TABLE IV. The baseline classification model employing Swin-B pretrained on ImageNet as its deep encoder demonstrates insufficient knowledge about driving scene identification. It fails in multi-label scene classification, only correctly identifying each scene with at most three attributes.

The foundation model, which assimilates knowledge regarding driving scene identification from diverse single-label datasets, significantly outperforms the baseline model that lacks such knowledge, correctly identifying scenes with respect to four to six attributes. However, an observable limitation of the foundation model is its frequent misidentification of dry road surface conditions as snowy, daytime as dawn, non-work zones as work zones, other road types as local roads, and non-intersection or three-way intersections as four-way intersections. For instance, the foggy weather condition in scenario (d) may have led the foundation model to erroneously classify daytime as dawn and dry road surfaces as snowy. Furthermore, the vehicle’s close proximity to the intersection makes it difficult to differentiate three-leg and four-leg features. Scenario (f) depicts an interstate highway that is slightly more complex than typical interstate driving scenes. The advertisement banner on the left and the open construction space on the right likely lead the model to misidentify it as a four-way intersection on a local road. Additionally, the atypical work zone features and the relatively farther distance of the

TABLE III  
PROGRESSIVE IMPROVEMENT IN TASK AND AVERAGE ACCURACIES (%) IN THE ABLATION STUDY

Model	KAA	CAL	ToD	Wea	RoF	WrR	Int	WrZ	GsI	Average
Baseline			17.1	13.2	12.7	53.1	42.1	53.3	64.6	36.6
Foundation	✓		73.9 <sup>56.8↑</sup>	65.8 <sup>52.6↑</sup>	73.0 <sup>60.3↑</sup>	55.3 <sup>2.2↑</sup>	48.1 <sup>6.0↑</sup>	66.4 <sup>13.1↑</sup>	92.8 <sup>28.2↑</sup>	67.9 <sup>31.3↑</sup>
with Adaptation	✓	✓(2 iters)	90.0 <sup>16.1↑</sup>	84.1 <sup>18.3↑</sup>	83.6 <sup>10.6↑</sup>	96.3 <sup>41.0↑</sup>	86.9 <sup>38.8↑</sup>	93.8 <sup>27.4↑</sup>	96.3 <sup>3.5↑</sup>	90.1 <sup>22.2↑</sup>
with Adaptation	✓	✓(5 iters)	<b>92.1</b> <sup>2.1↑</sup>	<b>90.9</b> <sup>6.8↑</sup>	<b>88.6</b> <sup>5.0↑</sup>	<b>97.1</b> <sup>0.8↑</sup>	<b>88.2</b> <sup>1.3↑</sup>	<b>94.2</b> <sup>0.4↑</sup>	<b>97.5</b> <sup>1.2↑</sup>	<b>92.7</b> <sup>2.6↑</sup>

ToD: Time of Day; Wea: Weather; RoF: Road Function; WrR: Weather-related Road Condition; Int: Intersection type; WrZ: Work Zone, GsI: Grade-separated Infrastructure.

TABLE IV  
GROUNDTRUTH AND PREDICTED LABELS FOR DRIVING SCENE IDENTIFICATION EXAMPLES

Example	Driving scene	Groundtruth	Predicted Labels			
			Baseline	Foundation	KAA-CAL (2 iters)	KAA-CAL (5 iters)
a		Night x Interstate Dry Non-intersection Non-work zone Open roads	Dawn x Collector Wet Non-intersection Work zone Open roads	Night x Local road Snowy Non-intersection Non-work zone Open roads	Night x Interstate Dry Non-intersection Non-work zone Open roads	Night x Interstate Dry Non-intersection Non-work zone Open roads
b		Daytime Overcast Arterial Dry 4-way Non-work zone Open roads	Dawn Snowing Collector Wet 3-way Work zone Open roads	Daytime Overcast Local road Snowy 4-way Work zone Open roads	Daytime Overcast Local road Dry 4-way Non-work zone Open roads	Daytime Overcast Arterial Dry 4-way Non-work zone Open roads
c		Daytime Overcast Local road Snowy 4-way Non-work zone Open roads	Dawn Snowing Arterial Snowy Non-intersection Work zone Open roads	Dawn Snowing Local road Snowy 4-way Non-work zone Open roads	Daytime Overcast Local road Snowy 4-way Non-work zone Open roads	Daytime Overcast Local road Snowy 4-way Non-work zone Open roads
d		Daytime Foggy Local road Dry 3-way Non-work zone Open roads	Dawn Snowing Collector Snowy Non-intersection Work zone Open roads	Dawn Foggy Local road Snowy 4-way Non-work zone Open roads	Daytime Foggy Local road Dry 3-way Non-work zone Open roads	Daytime Foggy Local road Dry 3-way Non-work zone Open roads
e		Daytime Clear Interstate Dry Non-intersection Non-work zone Overhead bridges	Dawn Snowing Collector Wet Non-intersection Work zone Open roads	Daytime Overcast Interstate Snowy Non-intersection Work zone Overhead bridges	Daytime Overcast Interstate Dry Non-intersection Non-work zone Overhead bridges	Daytime Clear Interstate Dry Non-intersection Non-work zone Overhead bridges
f		Daytime Clear Interstate Dry Non-intersection Work zone Open roads	Dawn Snowing Collector Snowy Non-intersection Work zone Open roads	Dawn Clear Local road Dry 4-way Non-work zone Open roads	Daytime Clear Arterial Dry Non-intersection Work zone Open roads	Daytime Clear Arterial Dry Non-intersection Work zone Open roads
g		Daytime Rainy Local road Wet Non-intersection Non-work zone Open roads	Dawn Clear Collector Snowy Non-intersection Work zone Open roads	Daytime Rainy Local road Wet 4-way Non-work zone Open roads	Dawn Rainy Local road Wet Non-intersection Non-work zone Open roads	Daytime Rainy Local road Wet Non-intersection Non-work zone Open roads

safety drums from the ego-vehicle fail the model in recognizing the work zone scenario. Overall, certain combinations of scene attribute labels are less prevalent in single-labeled datasets, thereby limiting the foundation model’s exposure and subsequent ability to accurately identify these specific scenes.

Utilizing feature proximity to recommend new training samples that are similar to the test data, CAL adapts the foundation model quickly to multitasking, demonstrating superior ability in classifying driving scenes comprehensively, as illustrated in the two rightmost columns in TABLE IV. Notably, the model adapted via CAL with only two iterations corrects most misclassifications in the foundation model, demonstrating the effectiveness of CAL. Meanwhile, with iterations up to five, the classification model learns the more fine-grained feature distributions, thus improving its ability

to identify driving scenes. For instance, in scenes a, b, d, and e, the foundation model misclassified the weather-related road condition as snowy. Assisted by CAL, now the adapted model can correctly recognize the category and reassign the class label. Furthermore, CAL mitigates dominant biases in feature distributions across single-label classification datasets. Specifically, in recognizing a four-way intersection, the model relies more on the complex behavior of traffic participants rather than on the actual geometric layout of the intersection (as seen in scenes c and g). CAL addresses this by providing additional class labels to supervise the learning of features that were previously either unseen or unaddressed in monotask learning.

### G. Comparison to SOTA Multitask Classification Models

In the end, the proposed KAA-CAL learning system was compared to SOTA methods. These models for comparison, which were reviewed in Section II-B, are now briefly summarized below.

- **ResNet18** [5]: A multitask model for scene classification that utilizes ResNet18 as a shared deep encoder was developed in [5]. It was applied to BDD100K for identifying Time of Day, Weather, and Scene Type.
- **ViT-B-16** [5]: ViT-B-16 is also used as a shared deep encoder for driving scene classification on BDD100K [5].
- **CF-NET** [6]: CF-NET utilizes ResNetV2-50 as the shared encoder and incorporates one 256-unit fully connected layer for each classifier. Single-label classifiers augment the multi-label classifier through feature fusion and stacking.
- **REC-NET** [4]: REC-NET employs EfficientNet-B2 as the shared encoder and lightweight task-specific classifiers that each consists of two fully connected layers.

To demonstrate the generalization of the KAA-CAL learning system, the comparative study was conducted on both BDD100K [10] and HSD [11]. BDD100K provides the opportunity for identifying three driving scene attributes, including Time of Day, Weather, and Scene Type. The HSD dataset includes class labels for four attributes: Intersection Type, Surface Condition, Driving Types, and Weather. Despite the limited number of attributes used for scene image labeling, these two datasets provide common benchmarks for objectively evaluating KAA-CAL against SOTA methods, whose performance is already reported. TABLE VI summarizes the sizes of these datasets in terms of training, validation, and testing partitions.

TABLE VI  
BDD100K AND HSD DATASETS

Dataset	Training	Validation	Testing
BDD100K	70,000	7,000	3,000
HSD*	53,115	5,500	2,275

\*Scene images were sampled every 100 frames from 80 hours of driving videos.

Our multitask classification model utilizes the foundation model as its deep encoder. It was subsequently trained via CAL to identify driving scenes in BDD100K and HSD, respectively, using a total of 15% of their training data over three iterations. In contrast, the four SOTA models, whose

encoders were pretrained on ImageNet, were trained on the full BDD100K and HSD training datasets, respectively. Results of the comparative study are summarized in TABLE V.

From TABLE V, it can be seen that KAA-CAL uses only 15% of the training data and achieves task accuracy comparable to SOTA methods that utilize all the training data. Specifically, on BDD100K, KAA-CAL achieves the same highest accuracy as ResNet18 and CF-NET in identifying Time of Day. KAA-CAL’s accuracy in identifying Weather (81.8%) exceeds the second-best method, CF-NET (81.0%), by 0.8%, and it slightly surpasses CF-NET by 0.1% in identifying Scene Type.

On HSD, KAA-CAL achieves the highest accuracy in identifying Surface Condition (91.1%), Driving Type (81.4%), and Weather (68.6%), exceeding the second best method by a small margin ranging from 0.1% to 0.3%. However, its accuracy in identifying Intersection Type (87.8%) is 1.2% below the best method, CF-NET (89.0%).

Importantly, Scene Type in BDD 100K and Driving Type in HSD are not attributes annotated in DSI. Therefore, the foundation model was not trained to recognize them. With the foundation model’s comprehensive knowledge of driving scene identification, and facilitated by CAL, the classification model efficiently gains the knowledge to identify driving scenes using these new attributes.

## VII. CONCLUSION

This paper introduced a new learning system called KAA-CAL, as well as the DSI dataset, to tackle multi-label driving scene classification, a challenging perception task for AVs. KAA acquires and accumulates knowledge about scene identification from the DSI dataset via monotask learning, improving the average classification accuracy by 31.3% compared to the baseline model pretrained on ImageNet. Subsequently, CAL resolves the domain shifts of feature and attribute distributions, boosting the performance to 92.7%. Additionally, achieving performance competitive with SOTA multitask models on BDD100K and HSD datasets while using only 15% of the training data highlights KAA-CAL’s generalization.

Several limitations are presented in this paper, which necessitate further investigation in future work. Primarily, due to resource constraints and a deliberate focus on methodological development, KAA-CAL was not evaluated on a broader range of datasets. Although AVs demand a more comprehensive approach to scene identification, this paper was dedicated to multi-label image classification, leaving perception tasks such as semantic segmentation and object detection to future

TABLE V  
CLASSIFICATION ACCURACY (%) COMPARISON WITH SOTA METHODS ON BDD100K AND HONDA HSD DATASET

	BDD100K			HSD			
	Time of Day	Weather	Scene Type	Intersection	Surface Condition	Driving Type	Weather
ResNet18 [5]	92.7	80.6	77.7	88.9	91.0	80.5	67.1
ViT-B-16 [5]	92.2	80.1	76.9	88.0	91.0	81.1	68.3
CF-NET [6]	92.7	81.0	78.5	<b>89.0</b>	90.8	78.2	66.7
RECNet [4]	92.6	80.2	76.7	87.0	90.4	80.7	68.0
KAA-CAL (ours)	<b>92.7</b>	<b>81.8</b>	<b>78.6</b>	87.8	<b>91.1</b>	<b>81.4</b>	<b>68.6</b>

exploration. Furthermore, despite its efficiency, CAL has not yet achieved the ideal few-shot model refinement for downstream tasks. Nevertheless, the work presented in this paper builds a foundation for further exploring these opportunities for improvement. Future study can also leverage the domain-specific prior and semantic guidance embedded in the driving scene identification model to advance video understanding and reasoning, and motion prediction for AVs.

#### ACKNOWLEDGMENT

Qin receives funding from the Rural Safe Efficient Advanced Transportation (R-SEAT) Center, a Tier-1 University Transportation Center (UTC) funded by the United States Department of Transportation (USDOT), through agreement number 69A3552348321. The contents of this paper reflect the views of the authors. USDOT assumes no liability for the contents or use thereof.

#### REFERENCES

- [1] V. Ramanishka, Y.-T. Chen, T. Misu, and K. Saenko, "Toward driving scene understanding: A dataset for learning driver behavior and causal reasoning," in *Proceedings of the IEEE Conference on Computer Vision and Pattern Recognition (CVPR)*, June 2018.
- [2] C. Sun, R. Zhang, Y. Lu, Y. Cui, Z. Deng, D. Cao, and A. Khajepour, "Toward ensuring safety for autonomous driving perception: Standardization progress, research advances, and perspectives," *IEEE Transactions on Intelligent Transportation Systems*, vol. 25, no. 5, pp. 3286–3304, 2024.
- [3] K. Muhammad, T. Hussain, H. Ullah, J. D. Ser, M. Rezaei, N. Kumar, M. Hijji, P. Bellavista, and V. H. C. de Albuquerque, "Vision-based semantic segmentation in scene understanding for autonomous driving: Recent achievements, challenges, and outlooks," *IEEE Transactions on Intelligent Transportation Systems*, vol. 23, no. 12, pp. 22 694–22 715, 2022.
- [4] M. Introvigne, A. Ramazzina, S. Walz, D. Scheuble, and M. Bijelic, "Real-time environment condition classification for autonomous vehicles," 2024. [Online]. Available: <https://arxiv.org/abs/2405.19305>
- [5] R. Prykhodchenko and P. Skruch, "Efficient multi-task learning for road scene classification: Scene, time, and weather predictions," in *2024 IEEE 20th International Conference on Intelligent Computer Communication and Processing (ICCP)*, 2024, pp. 1–7.
- [6] T. T. Duong, T. P. Nguyen, and J. W. Jeon, "Combined classifier for multi-label network in road scene classification," in *2020 IEEE International Conference on Consumer Electronics - Asia (ICCE-Asia)*, 2020, pp. 1–4.
- [7] L. Chen, W. Zhan, W. Tian, Y. He, and Q. Zou, "Deep integration: A multi-label architecture for road scene recognition," *IEEE Transactions on Image Processing*, vol. 28, no. 10, pp. 4883–4898, 2019.
- [8] F. Wu, "Wz-traffic dataset," <https://github.com/Fangyu0505/traffic-scene-recognition>, 2019.
- [9] I. Admin, A. Ghosh, R. Tamburo, S. Narasimhan, S. Zheng, J. A. Padilla, M. Cardei, N. Dunn, and H. Zhu, "ROADWork Data," 7 2024. [Online]. Available: [https://kilthub.cmu.edu/articles/dataset/ROADWork\\_Data/26093197](https://kilthub.cmu.edu/articles/dataset/ROADWork_Data/26093197)
- [10] F. Yu, H. Chen, X. Wang, W. Xian, Y. Chen, F. Liu, V. Madhavan, and T. Darrell, "Bdd100k: A diverse driving dataset for heterogeneous multitask learning," in *Proceedings of the IEEE/CVF conference on computer vision and pattern recognition*, 2020, pp. 2636–2645.
- [11] A. Narayanan, I. Dwivedi, and B. Dariush, "Dynamic traffic scene classification with space-time coherence," in *2019 International Conference on Robotics and Automation (ICRA)*. IEEE, 2019, pp. 5629–5635.
- [12] F. Wu, S. Yan, J. S. Smith, and B. Zhang, "Deep multiple classifier fusion for traffic scene recognition," *Granular Computing*, vol. 6, no. 1, pp. 217–228, 2021.
- [13] R. Prykhodchenko and P. Skruch, "Road scene classification based on street-level images and spatial data," *Array*, vol. 15, p. 100195, 2022. [Online]. Available: <https://www.sciencedirect.com/science/article/pii/S2590005622000467>
- [14] J. Ni, K. Shen, Y. Chen, W. Cao, and S. X. Yang, "An improved deep network-based scene classification method for self-driving cars," *IEEE Transactions on Instrumentation and Measurement*, vol. 71, pp. 1–14, 2022.
- [15] M. Cordts, M. Omran, S. Ramos, T. Rehfeld, M. Enzweiler, R. Benenson, U. Franke, S. Roth, and B. Schiele, "The cityscapes dataset for semantic urban scene understanding," in *Proc. of the IEEE Conference on Computer Vision and Pattern Recognition (CVPR)*, 2016.
- [16] A. Geiger, P. Lenz, C. Stiller, and R. Urtasun, "Vision meets robotics: The kitti dataset," *International Journal of Robotics Research (IJRR)*, 2013.
- [17] H. Caesar, V. Bankiti, A. H. Lang, S. Vora, V. E. Liong, Q. Xu, A. Krishnan, Y. Pan, G. Baldan, and O. Beijbom, "nuscenes: A multimodal dataset for autonomous driving," *arXiv preprint arXiv:1903.11027*, 2019.
- [18] J. Gou, B. Yu, S. J. Maybank, and D. Tao, "Knowledge distillation: A survey," *International Journal of Computer Vision*, vol. 129, no. 6, pp. 1789–1819, 2021.
- [19] A. Romero, N. Ballas, S. E. Kahou, A. Chassang, C. Gatta, and Y. Bengio, "Fitnets: Hints for thin deep nets," *arXiv preprint arXiv:1412.6550*, 2014.
- [20] D. Ma, J. Pang, M. B. Gotway, and J. Liang, "Foundation ark: Accruing and reusing knowledge for superior and robust performance," in *Medical Image Computing and Computer Assisted Intervention – MICCAI 2023*, H. Greenspan, A. Madabhushi, P. Mousavi, S. Salcudean, J. Duncan, T. Syeda-Mahmood, and R. Taylor, Eds. Cham: Springer Nature Switzerland, 2023, pp. 651–662.
- [21] G. M. Van de Ven, H. T. Siegelmann, and A. S. Tolias, "Brain-inspired replay for continual learning with artificial neural networks," *Nature communications*, vol. 11, no. 1, p. 4069, 2020.
- [22] X. Zhan, Q. Wang, K. hao Huang, H. Xiong, D. Dou, and A. B. Chan, "A comparative survey of deep active learning," 2022. [Online]. Available: <https://arxiv.org/abs/2203.13450>
- [23] D. Yoo and I. S. Kweon, "Learning loss for active learning," in *Proceedings of the IEEE/CVF Conference on Computer Vision and Pattern Recognition (CVPR)*, June 2019.
- [24] O. Sener and S. Savarese, "Active learning for convolutional neural networks: A core-set approach," 2018. [Online]. Available: <https://arxiv.org/abs/1708.00489>
- [25] A. Hekimoglu, M. Schmidt, and A. Marcos-Ramiro, "Active learning with task consistency and diversity in multi-task networks," in *Proceedings of the IEEE/CVF Winter Conference on Applications of Computer Vision (WACV)*, January 2024, pp. 2503–2512.
- [26] L. Schmidt, S. Santurkar, D. Tsipras, K. Talwar, and A. Madry, "Adversarially robust generalization requires more data," in *Advances in Neural Information Processing Systems*, S. Bengio, H. Wallach, H. Larochelle, K. Grauman, N. Cesa-Bianchi, and R. Garnett, Eds., vol. 31. Curran Associates, Inc., 2018. [Online]. Available: [https://proceedings.neurips.cc/paper\\_files/paper/2018/file/f708f064faaf32a43e4d3c784e6af9ea-Paper.pdf](https://proceedings.neurips.cc/paper_files/paper/2018/file/f708f064faaf32a43e4d3c784e6af9ea-Paper.pdf)
- [27] Z. Liu, Y. Lin, Y. Cao, H. Hu, Y. Wei, Z. Zhang, S. Lin, and B. Guo, "Swin transformer: Hierarchical vision transformer using shifted windows," in *Proceedings of the IEEE/CVF international conference on computer vision*, 2021, pp. 10 012–10 022.
- [28] A. Tarvainen and H. Valpola, "Mean teachers are better role models: Weight-averaged consistency targets improve semi-supervised deep learning results," *Advances in neural information processing systems*, vol. 30, 2017.
- [29] M. Mermillod, A. Bugaiska, and P. Bonin, "The stability-plasticity dilemma: Investigating the continuum from catastrophic forgetting to age-limited learning effects," p. 504, 2013.
- [30] G. Wu, S. Gong, and P. Li, "Striking a balance between stability and plasticity for class-incremental learning," in *Proceedings of the IEEE/CVF International Conference on Computer Vision (ICCV)*, October 2021, pp. 1124–1133.
- [31] M. De Lange, R. Aljundi, M. Masana, S. Parisot, X. Jia, A. Leonardis, G. Slabaugh, and T. Tuytelaars, "A continual learning survey: Defying forgetting in classification tasks," *IEEE Transactions on Pattern Analysis and Machine Intelligence*, vol. 44, no. 7, pp. 3366–3385, 2022.
- [32] J. Deng, W. Dong, R. Socher, L.-J. Li, K. Li, and L. Fei-Fei, "Imagenet: A large-scale hierarchical image database," in *2009 IEEE Conference on Computer Vision and Pattern Recognition*, 2009, pp. 248–255.
- [33] X. Glorot and Y. Bengio, "Understanding the difficulty of training deep feedforward neural networks," in *Proceedings of the Thirteenth International Conference on Artificial Intelligence and Statistics*, ser. Proceedings of Machine Learning Research, Y. W. Teh and M. Titterton, Eds., vol. 9. Chia Laguna Resort, Sardinia,

Italy: PMLR, 13–15 May 2010, pp. 249–256. [Online]. Available: <https://proceedings.mlr.press/v9/lorot10a.html>

- [34] V. Sundharam, A. Sarkar, A. Svetovidov, J. S. Hickman, and A. L. Abbott, “Characterization, detection, and segmentation of work-zone scenes from naturalistic driving data,” *Transportation Research Record*, vol. 2677, no. 3, pp. 490–504, 2023. [Online]. Available: <https://doi.org/10.1177/03611981221115724>
- [35] J. Shen, W. Yan, P. Li, and X. Xiong, “Deep learning-based object identification with instance segmentation and pseudo-lidar point cloud for work zone safety,” *Computer-Aided Civil and Infrastructure Engineering*, vol. 36, no. 12, pp. 1549–1567, 2021. [Online]. Available: <https://onlinelibrary.wiley.com/doi/abs/10.1111/mice.12749>



**Ke Li** (Graduate Student Member, IEEE) received the B.S. degree in transportation from Southeast University, China, in 2021, and the M.S. degree in Civil Engineering from University of Illinois Urbana-Champaign, IL, USA, in 2023. He is currently pursuing the Ph.D. degree in the Department of Civil Engineering at Stony Brook University, NY, USA. He has been a research assistant since 2023, working on perception and recognition for autonomous driving systems and intelligent systems using deep learning methods.



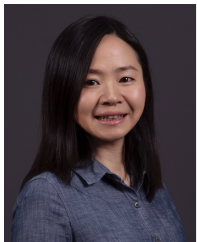
**Chenyu Zhang** (Graduate Student Member, IEEE) received the B.S. degree in Bridge Engineering in 2018 and the M.S. degree in Civil Engineering in 2021, both from the School of Highway, Chang'an University, Xi'an, China. He is currently pursuing the Ph.D. degree in Civil Engineering at Stony Brook University, Stony Brook, NY, USA. His research interests include intelligent transportation systems, transportation asset management, and resilient infrastructure systems.



**Yuxin Ding** received his Bachelor degree from the Civil Aviation University Of China, and Master degree from Georgia Institute Of Technology. He is currently pursuing the Ph.D. with the Department of Civil and Environmental Engineering, Penn State University, Pennsylvania, USA. His research is focused on autonomous vehicles and dynamic system modeling.



**Xianbiao Hu** received the B.Eng. and M.Eng. degrees in Transportation Engineering from Tongji University, China, and the Ph.D. degree in Transportation Engineering from the University of Arizona, USA. His research focuses in the area of Smart Mobility System, Dynamic System Modeling, Vehicle Technology, Active Demand Management, Automated Vehicles, and Transportation Electrification.



**Ruwen Qin** (Member, IEEE) received the B.E. and M.S. degrees in spacecraft design from Beijing University of Aeronautics and Astronautics and the Ph.D. degree in industrial engineering & operations research from Pennsylvania State University. She is an Associate Professor of civil engineering at Stony Brook University. Her research is focused on sensing and deep learning methods to build perception and cognition abilities for intelligent systems like autonomous vehicles. She is a member of IEEE Intelligent Transportation Systems Society.